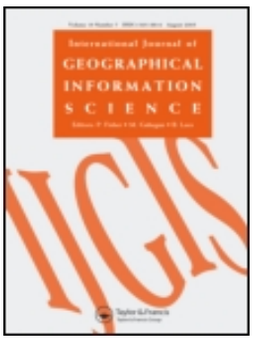

International Journal of Geographical Information Science

ISSN: 1365-8816 (Print) 1362-3087 (Online) Journal homepage: http://www.tandfonline.com/loi/tgis20

Visualizing and quantifying the movement of vegetative drought using remote-sensing data and GIS

Coco M. Rulinda , Alfred Stein & Ulan D. Turdukulov

To cite this article: Coco M. Rulinda , Alfred Stein & Ulan D. Turdukulov (2013) Visualizing and quantifying the movement of vegetative drought using remote-sensing data and GIS, International Journal of Geographical Information Science, 27:8, 1481-1496, DOI: 10.1080/13658816.2012.723712

To link to this article: http://dx.doi.org/10.1080/13658816.2012.723712

International Journal of Geographical Information Science, 2013
Vol. 27, No. 8, 1481–1496, http://dx.doi.org/10.1080/13658816.2012.723712

Taylor & Francis
Taylor & Francis Group

Visualizing and quantifying the movement of vegetative drought using remote-sensing data and GIS

Coco M. Rulinda*, Alfred Stein and Ulan D. Turdukulov

Faculty of Geo-Information Science and Earth Observation (ITC), University of Twente, Enschede, The Netherlands

(*Received 13 December 2011; final version received 19 August 2012*)

Remote-sensing-based drought monitoring methods provide fast and useful information for a sustainable management strategy of drought impact over a region. Common pixel-based monitoring methods are limited in the analysis of the dynamics of this impact at regional scale. For instance, these hardly allow us to quantify the movement of drought in space and time and to compare drought with rainfall deficits without losing the variability of these events within a region. This study proposed an object-based approach that allowed us to visualize and quantify the spatio-temporal movement of drought impact on vegetation, called vegetative drought, in a region. The GIS software Dynomap was used to extract and track objects. Measures of distance and angle were used for determining the speed and direction of vegetative drought and rainfall deficit objects, calculated from the National Oceanic and Atmospheric Administration's (NOAA's) normalized difference vegetation index and rainfall estimates data. The methods were applied to the two rainy seasons during the drought year 1999 in East Africa. Results showed that vegetative drought objects moved into the southwestern direction at an average angle of −138.5° during the first season and −144.5° during the second season. The speed of objects varied between 38 km dekad^{-1} and 185 km dekad^{-1} during the first season and between 33 km dekad^{-1} and 144 km dekad^{-1} during the second season, reflecting the rate of spread between dekads. Vegetative drought objects close to rainfall deficit objects showed similar trajectories and sometimes regions overlapped. This indicated that the two events are related. We conclude that a spatiotemporal relationship existed between the two types of events and that this could be quantified.

Keywords: drought; trajectories; spatio-temporal objects; spatial data quality; remote sensing; GIS

1. Introduction

Drought is defined as a period drier than normal conditions. It is a natural and recurrent phenomenon that affects various regions of the World such as East Africa. In recent years, geographic information science (GIS) and remote sensing (RS) have played a major role in studying drought (Mokhtari *et al.* 2011, Murad and Islam 2011) and its impact on vegetation using indices such as the normalized difference vegetation index (NDVI) (Tucker 1979, Davenport and Nickolson 1993, Eklundh 1996, 1998, Nicholson *et al.* 1999). This is done on the basis of the primary understanding of vegetative drought as a period during

*Corresponding author. Email: coco.rulinda@gmail.com

which vegetation health is below normal. In this article, vegetative drought is defined as the negative departure of the current NDVI values from their corresponding long-term mean values. As drought develops and intensifies, the impact on vegetation spreads throughout a region. Analyzing the spatiotemporal movements of vegetative drought can improve our understanding of the phenomenon and help in planning to reduce its devastating effects.

Issues of geospatial data quality have been addressed, and the vague characterization of vegetative drought was modeled using a fuzzy classification approach (Rulinda *et al.* 2012). These advancements allowed us to quantify the dynamics of vegetative drought with measures of certainties, but without providing an understanding of the spatiotemporal movement of vegetative drought at a regional scale. Advancements have also been made during the past years in the development of object-based image analysis (Jong *et al.* 2001, Blaschke *et al.* 2008, Stein *et al.* 2009, Blaschke 2010, Blaschke *et al.* 2011, Mokhtari *et al.* 2011). A major difference between pixel-based and object-based image analyses is that object-based approaches provide output in the form of thematic maps that are composed of geographical entities. Relationships between these entities can be quantified and visualized. Visualization techniques to explore spatial data have been widely discussed (e.g., Kraak and MacEachren 1999).

In this study, we propose a method to visualize and quantify the spatiotemporal movement of vegetative drought over East Africa using NDVI data. Spatial relationships of vegetative drought regions with rainfall deficit regions are assessed.

2. Materials and methods

2.1. Study area and period

The study area covers a subset of East Africa including Burundi, Kenya, Rwanda, Tanzania, and Uganda, as in Rulinda *et al.* (2012). In this article, the drought year 1999 was analyzed for the two main rainy seasons. The United Nations International Children's Emergency Fund (UNICEF) reported a serious drought that developed in East Africa since early that year (UNICEF 2000). The Food and Agricultural Organization (FAO) also reported serious crop failures in several regions of Tanzania in November 1999 (FAO 1999). In Kenya, significant harvest shortfalls were forecast during the same period in several parts due to drought, and worsening nutritional conditions were reported in pastoral and agro-pastoral areas (FAO 1999). During the same period, in Burundi and Rwanda, inadequate rainfall affected the crops.

2.2. Data and processing

2.2.1. Characterizing vegetative drought

In this study, we used the National Oceanic and Atmospheric Administration's (NOAA's) Advanced Very High Resolution Radiometer- (AVHRR-) derived 10-day (dekad) NDVI products, processed by the Global Inventory Monitoring and Modeling Systems (GIMMS) group (Tucker *et al*. 2005, Pinzón *et al.* 2005) at the US National Aeronautic Space Agency (NASA/Goddard Space Flight Center (GSFC)). Data from March to May 1999 and from October 1999 to January 2000 and their corresponding long-term mean values were used. The characteristics of these data can be found in Tucker *et al.* (2005) and Pinzón *et al.* (2005). We used the Global Land Cover 2000 (GLC2000) (JRC-GEMU 2000) map to mask out non-vegetated areas and forests. Three classes according to the GLC2000 Africa-v5-legend were selected: (7) mosaic forest/croplands, (18) croplands (>50% of pixel area), and (19) croplands with open woody vegetation.

Vegetative drought was characterized from the difference NDVI images, using a fuzzy classification in a similar way as in Rulinda *et al.* (2012). Vegetative drought images, called vd images, resulting from this classification process, have pixels with $d(x)$ values ranging between 0 (i.e., no drought membership) and 1 (i.e., full drought membership).

The fuzzy classification results in fuzzy-fuzzy image regions. These are field data models that do not allow us to quantify certain spatiotemporal relations between different entities. An object-field data model is then used instead. The object-field is an ontology of geographic phenomena that allows to represent and model fuzzy phenomena, as well as reasoning about them. The fuzzy-fuzzy image regions have two non-overlapping classes: drought and non-drought, and we are interested in all areas possibly affected by drought. Hence, the fuzzy-fuzzy image regions are formalized into fuzzy objects with crisp boundaries, called crisp-fuzzy objects. The formalization process is explained in Section 2.3.

2.2.2. Characterizing rainfall deficit

To further assess the relationship between vegetative drought and rainfall deficit, rainfall estimates (RFE) image data covering the same area in East Africa were used. These data were obtained from NOAA's Climate Prediction Center (Xie and Arkin 1997). Characterisctics of these data can be found in Xie and Arkin (1997). As vegetation health has a lagged response to rainfall, we have selected an RFE period longer than that for the NDVI images in order to capture their relationship. Images from January to May and from September to December 1999 were used. Cumulative RFE values were obtained for each dekad by adding up values from previous dekads.

RFE anomaly values for each pixel, denoted by *ra*, were calculated as the difference between the current RFE and the long-term mean values, denoted by $\overline{RFE}$. Values of *ra* vary between $\times 250$ and 250 mm. Rainfall deficit values, denoted by *rd*, were obtained from *ra* values by

$$rd = \begin{cases} 0 & \text{if} \quad ra \geq 0 \\ \frac{-ra}{2.5} & \text{if} \quad ra < 0 \end{cases}$$

Values of *rd* thus vary between 0, no deficit, and 100, maximum deficit. Rainfall deficit images were used as input to extract and track rainfall deficit objects.

2.3. Extracting objects

In this study, we call an *entity* the set of interconnected pixels with positive values, and an *object* the set of entities linked in time. Cheng *et al.* (1997) proposed methods to identify fuzzy objects from field observations. According to their definitions, vegetative drought entities can be characterized in space as objects with crisp boundaries and fuzzy interiors, called crisp-fuzzy objects. The formalization approach used in this article for the crisp-fuzzy object model differs from the one proposed by Cheng *et al.* (1997). Assuming that $d(x)$ represents the membership value of grid cell P with respect to vegetative drought class, and D[P,d] represents the decision function assigning P to a region of vd, we created conditional boundaries by assigning pixels with $d(x) > 0$ to the vegetative drought class as follows:

$$\begin{aligned} \mathrm{D}[\mathrm{P}, d] &= 1 \quad \text{if } d(x) \geq 0 \\ \mathrm{D}[\mathrm{P}, d] &= 0 \quad \text{if } d(x) = 0 \end{aligned}$$

A similar formalization process is applied to indentify *rd* entities from *rd* images. Assuming that $r(x)$ represents the membership value of grid cell P with respect to rainfall deficit class, and D[P,*r*] represents the decision function assigning P to a region of *rd*, we created conditional boundaries by assigning all pixels with $r(x) > 0$ to the rainfall deficit class as follows:

$$\begin{aligned} \mathrm{D}[\mathrm{P}, r] &= 1 \quad \text{if } r(x) \geq 0 \\ \mathrm{D}[\mathrm{P}, r] &= 0 \quad \text{if } r(x) = 0 \end{aligned}$$

The prototype *Dynomap* developed by Turdukulov *et al.* (2005, 2007) in ENVI/IDL® is used to extract and visualize the evolution of entities in RS images. Entities are extracted with the following attributes:

- The *time t*, representing the image frame, in this case, dekad;
- The *entity ID* that uniquely identifies an object at time *t*;
- The *support-area*, or the spatial coverage of the entity, calculated as in Equation (5) of Rulinda *et al.* (2012) and the *mean-area* of the entity, calculated as in Equation (7) of Rulinda *et al.* (2012)
- The *centroid*, or *center of mass* of entities are used to visualize the evolution of objects in space and time. The coordinates of the *centroid*, C_x and C_y, are calculated for each entity as in Equations (9) and (10) of Rulinda *et al.* (2012).

As centroids are given in (*x,y*) image coordinates, a common linear transformation is applied as follows: $\mathrm{Lat} = (C_y) \cdot (\mathrm{Top} - \mathrm{Bottom})/(\mathrm{MaxRow} + \mathrm{Bottom})$ and $\mathrm{Lon} = (C_x) \cdot (\mathrm{Right} - \mathrm{Left})/(\mathrm{MaxCol} + \mathrm{Left})$, where we used the following values: $\mathrm{Top} = 4.63$, $\mathrm{Bottom} = -11.77$, $\mathrm{MaxRow} = 224$, $\mathrm{MaxCol} = 179$, $\mathrm{Right} = 41.92$ and $\mathrm{Left} = 28.81$.

Due to the spatial distribution of positive *rd* pixels in some dekadal images, threshold values were chosen to separate the interconnected patches observed on the *rd* images. These values were selected manually by selecting the maximum value of pixel that could visually separate exclusive patches, for each dekad. For the first season, the *rd* values of 27, 10, 8, 27, 20, 46, 29, and 33 were used for the dekads of Jan I, Jan II, Jan III, Feb I, Feb II, Feb III, Mar I, and Mar II, respectively. For the second season, the *rd* values of 2, 6, 11, 22, 7, 68, and 78 were used for Oct I, Oct II, Oct III, Nov I, Nov II, Dec II, and Dec III, respectively.

2.4. Tracking objects

Dynomap uses the post-processing method originally proposed by Samtaney *et al.* (1994) and later modified by Silver and Wang (1996) to track objects. The post-processing method allows one to handle deformable dynamic phenomena. It can handle objects with crisp boundaries and fuzzy interiors. After objects are extracted in each image, that is, as entities, they are grouped to form objects in time using the spatial overlap criterion. Details on the tracking algorithm can be found in Turdukulov (2006). Uniquely labeled entities, by means of a set of relations, form a compound entity called an object. Each object has an `object ID` that uniquely identifies it. Samtaney *et al.* (1994) introduced a number of evolutionary events that describe the creation, continuation, and dissipation of objects, as illustrated in Figure 1.

When an entity appears in an image, an object is created. Object creation can also result from the splitting or merging of existing objects at previous time. Splitting and merging

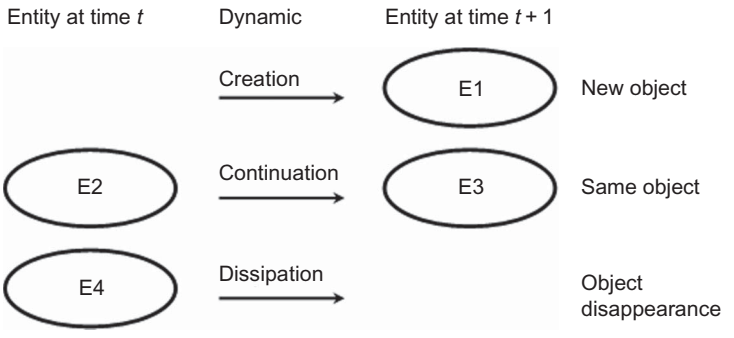

Figure 1. Spatiotemporal dynamics of objects represented by uniquely labeled entities E.

happen when there is no minimum overlap allowing to link the image entity at time t to the one at time $t + 1$. Objects can dissipate by merging with other objects, resulting in the creation of a new object. Visualizing centroids rather than the regions of entities in a 3D space–time cube allows one to better understand the movement of objects in a time series. The size of the centroids can indicate the spatial coverage or the intensity of an entity K; hence, the evolution of spatial attributes of an object can also be observed in the 3D space–time cube.

Quantifying the spatial relations between entities is important to analyze the movement of an object. Spatiotemporal relations can exist between entities of the same or different objects. In this study, we first analyzed relations between entities of the same object. Centroids indicate the core locations of the entities, and the distance d between the centroids of an entity K_1 at time t and an entity K_2 at time $t + 1$ was calculated using the Haversine formula. This formula gives the great-circle distance between two points on a surface of a sphere in kilometers (Sinnot 1984). It was used in this study to obtain the distance d between the Lat and Lon coordinates of the centroids of two entities as

$$
\begin{aligned}
a &= \sin^2\left(\frac{\Delta\mathrm{Lat}}{2}\right) + \cos(\mathrm{Lat}_1) \times \cos(\mathrm{Lat}_2) \times \sin^2\left(\frac{\Delta\mathrm{Lon}}{2}\right) \\
c &= 2 \cdot a \tan 2\left(\sqrt{y}, \sqrt{x}\right) \\
d &= R \times c
\end{aligned}
$$

where ΔLat and ΔLon are the differences between the Lat and Lon coordinates of the two centroids, respectively, Lat_1 and Lat_2 are the latitude of the first and second centroids, respectively, and $R = 6.371$ km is the Earth's radius. The function $a\tan 2(y, x)$ is the angle in radians between the positive x-axis of a plane and the point given by the coordinates (x, y) on the plane. The distance between the centroids of entities is hence referred to as the distance between entities.

The speed v of movement of vegetative drought from time t to time $t + 1$ was obtained from the distance divided by the time and expressed in km dekad^{-1}. The direction of movement of a vegetative drought object from time t to time $t + 1$ was calculated using the angle θ between the lines defined by the locations of the two centroids of entities K_1 and K_2 at time t and $t + 1$, respectively, and the horizontal axis. It is given in degrees by:

$$
\theta(k_1, k_2) = a\tan 2(C_y(K_2) - C_y(K_1), C_x(K_2) - C_x(K_1))\frac{180}{\pi}
$$

Values between 0° and 90° indicate a movement toward East–North; values between 90° and 180° indicate a movement toward North–West. Values between 0° and −90° indicate a movement toward East–South, whereas values between −90° and −180° indicate a South–West movement.

2.5. Assessing relationship between **vd** *and* **rd** *objects*

The relationship between vegetative drought and rainfall deficit objects, denoted `vd` and `rd`, respectively, can be assessed qualitatively by visually comparing the trajectories of both sets of objects and quantitatively by measuring the distances between them, or by assessing their region overlapping in the space–time cube.

For the visual approach, the Lat and Lon coordinates of objects were plotted separately per season, and the trajectories were compared. Furthermore, both sets of images were input into Dynomap, after creating alternated stacked layers in ENVI®, in order to assess their overlapping. For this study, stacks of 24 layers were created for each season following the chronological order of image frames. For the first season, the first seven layers are rainfall deficit images from Jan I to Mar I, followed by an alternance between vegetative drought images and rainfall deficit images until May III. For the second season, the first four layers are rainfall deficit images, followed by an alternance between vegetative drought images and rainfall deficit images until Dec III. The stacked layers ended with three layers of vegetative drought until Jan III.

For the quantitative approach, the distances *d* between the centroids of the entities of selected objects from different sets visually close to each other were calculated.

3. Results

3.1. Vegetative drought objects

The trajectories of all extracted `vd` objects are shown in Figures 2c and d and 3c and d. For the first season (Figure 2), 128 `vd` objects were extracted, whereas for the second season (Figure 3), 215 `vd` objects were extracted.

In Figures 2c and d, the existence of the `vd` object `vd1` (in blue) is observed in March 1999, in northern Tanzania. From April onwards, the object shifts toward the south and its size, that is, *support-area*, decreases before the object dissipates at the second dekad of May. A smaller object `vd77` (in purple) is observed from April 1999 through the end of the season in northern Kenya, shifting slightly toward the center. In Figure 2c and d, we observe a vegetative drought object `vd24` (in green) starting in eastern Kenya and shifting south toward the center of Tanzania. Another vegetative drought object `vd115` (in dark blue) smaller than the first one is also observed in the northeastern part of Kenya from the end of October to the end of November. These large objects are also shown in Figure 4a `vd1`, c `vd77`, (b) `vd24`, and (d) `vd115`.

The change of the size of centroids indicates the change in the *support-area* or spatial coverage, that is, shrinkage or expansion of the objects. The shifting of the centroids indicates either that the intensity of the object has moved to another area of the entity, the entities have shifted, or a combination of the above. In the next section, we analyze these dynamics.

3.2. Dynamics of **vd** *objects*

Distances and angles between the centroids of entities of the same object are calculated. Object `vd1`, with a average speed of 185 km dekad^{-1} moves faster than `vd77` with an

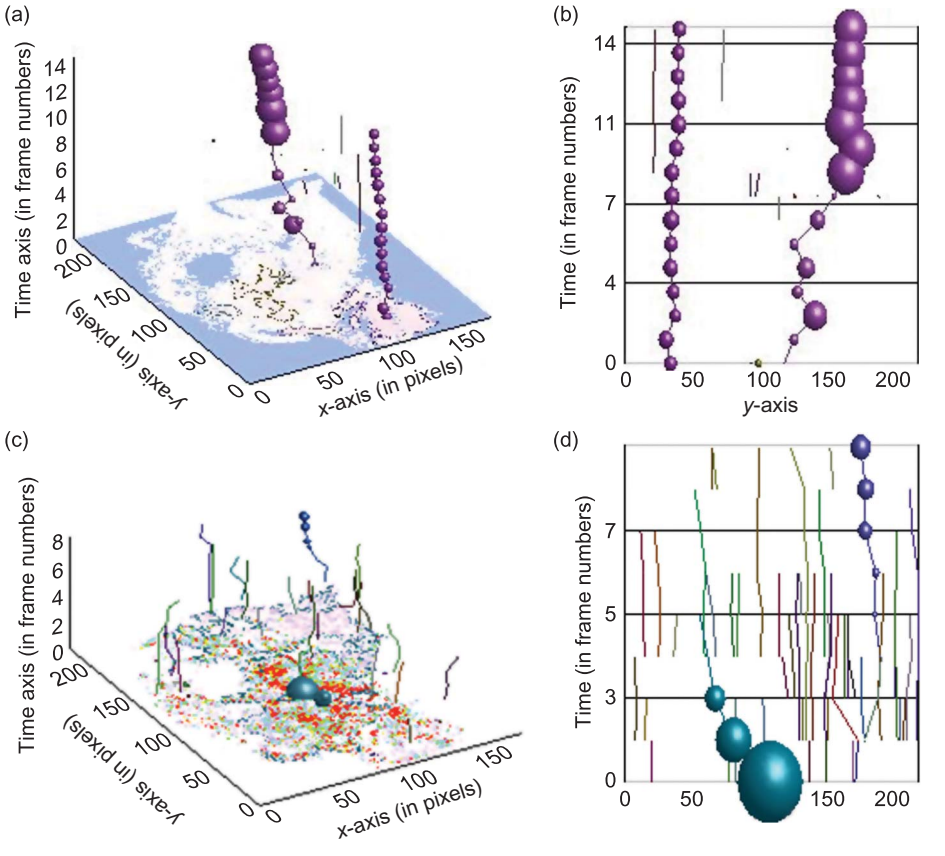

Figure 2. Trajectories of rd objects in (a) 3D space–time cube and (b) 2D along the *y*-axis (South–North) and vd objects in (c) 3D space–time cube and (d) 2D along the *y*-axis (South–North), for the first season.

Notes: Different colors represent different objects and different sizes represent different values of support-area of objects. Frame numbers on the time axis represent sequence numbers of dekads.

average speed of 38 km dekad^{-1} and object `vd24` with an average speed of 144 km dekad^{-1} moves faster than `vd115` with an average speed of 33 km dekad^{-1}. When considering `vd24` at the time interval between the third dekad of October and the first dekad of November, the speed of movement equals to 674 km dekad^{-1}, whereas from the first to the second dekad of November it is 33 km dekad^{-1}.

The directions of the movement of `vd` objects are calculated as angles considering the locations of the centroids at the appearance and last existence of the object. Object `vd1` moved at −124°, `vd77` at −153°, `vd24` at −118°, and `vd115` at −171°. These values indicate that vegetative drought, from these four objects, moved into the southwestern direction from its origin.

3.3. Rainfall deficit objects

Rainfall deficit objects, denoted `rd`, were extracted from rainfall deficit images. The locations of the centroids of the largest extracted objects are shown in Figure 2a and

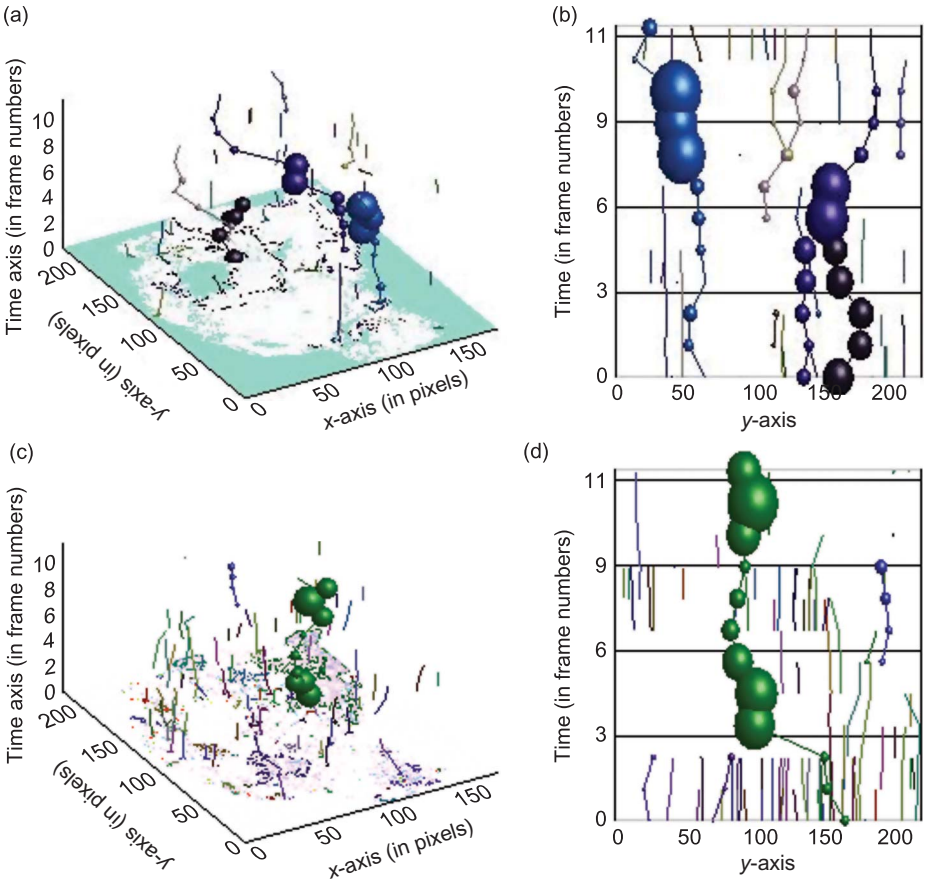

Figure 3. Trajectories of rd objects in (a) 3D space–time cube and (b) 2D along the *y*-axis (South–North) and vd objects in (c) 3D space–time cube and (d) 2D along the *y*-axis (South–North) for the second season.

Notes: Different colors represent different objects and different sizes represent different values of support-area of objects. Frame numbers on the time axis represent sequence numbers of dekads.

b for the first season and in Figure 3a and b for the second season. For the first season, 38 `rd` objects were extracted, whereas for the second season, 78 `rd` objects were extracted.

Two large `rd` objects are observed for the first season, and six large objects are observed for the second season. For the first season, object `rd1` is persisting in southeastern Tanzania, whereas object `rd8`, originating in southern Kenya, moved and persisted in northern Kenya (Figure 2a and b). During the second season, we observe more objects that are clustered in southern Tanzania, in Kenya, and in Uganda. These regions coincide with regions of vegetative drought. These objects also show different spatiotemporal dynamics. During the first season, we observe two large objects; one starting and ending in southeastern Tanzania, whereas the other starts in southern Kenya and ends in northern Kenya. They both have the same duration; however, one `rd2` is more stable (persistent) in space than `rd8`.

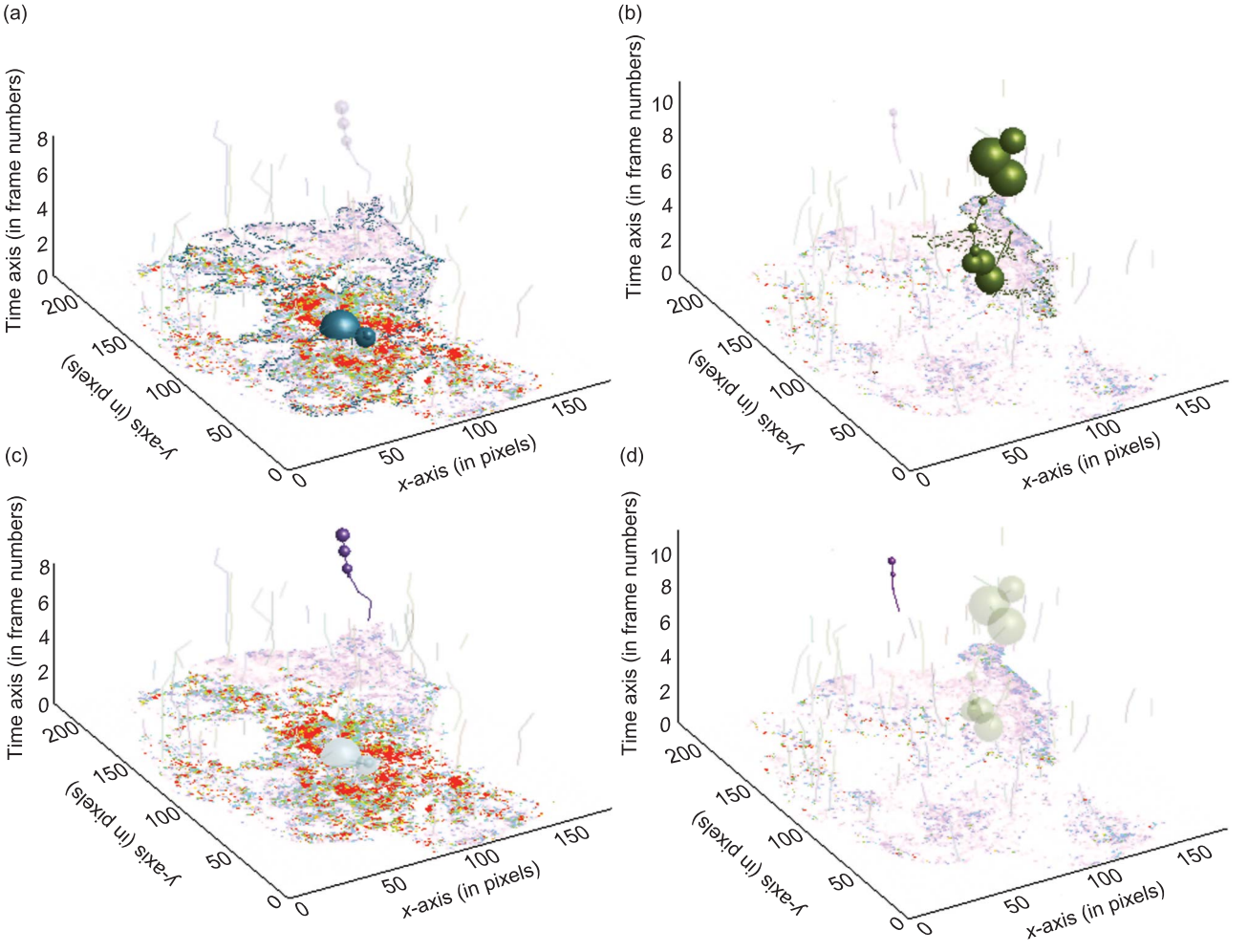

Figure 4. Trajectories of two selected vd objects in 3D space–time cube for (a) vd1 and (b) vd77 for the first season and (c) vd24 and (d) vd115 for the second season.

Notes: Different colors represent different objects and different sizes represent different support-area values of objects. Frame numbers on the time axis represent sequence numbers of dekads.

3.4. *Dynamics of* rd *objects*

Distances and angles between the centroids for each rd were calculated for each season, respectively. During the first season, object rd1 moved at an average speed of 20 km dekad^{-1} and 129.76°, whereas object rd8 moved at an average speed of 76 km dekad^{-1} and at an average angle of 102.66°. For the second season, object rd8 moved at an average of 77 km dekad^{-1} and −70.93°, rd9 at 76 km dekad^{-1} and 141.78°, rd10 at 88 km dekad^{-1} and −27.29°, rd45 at 78 km dekad^{-1} and 120.44°, rd50 at 56 km dekad^{-1} and −29.55°, and rd52 at 29 km dekad^{-1} and 157°.

We observe that objects rd1 and rd8 in the first season and objects, rd9, rd45, and rd52 in the second season moved into the northwestern direction from their origin. Objects rd8, rd10 and rd50 moved into the southeastern direction from their locations of origin. Although some objects present the same direction of movement, results must be interpreted with care along with the speed of movement for a complete understanding.

3.5. *Relationship between* vd *and* rd *objects*

Trajectories of objects are plotted together by season, along the Lat and Lon axes, as shown in Figures 5 and 6. Note that vd objects are observed from March and October for the first and second seasons, respectively, and rd objects are observed from January and September for the first and second seasons, respectively. Hence, we compare the largest objects at the time of their co-existence. Results show similar trajectories of vd and rd objects, indicating that persisting rainfall deficit in certain areas have caused vegetative drought.

For the first season (Figure 5), we observe that vd1 trajectory along the *Lat* direction is close to rd8, whereas vd77 was closer to rd8 at the first dekad of March and moved toward rd2. Object vd1 may have been influenced first by rd8 and later on by rd2. Results indicate that the distance between vd1 and rd8 increased from 298 to 1094 km through time, whereas between vd1 and rd2, it decreases from 641 to 512 km. This quantitatively indicates that vegetative drought object vd1 may have been influenced first by rd8 and later by rd2. The distance between vd77 and rd8 also decreased from 389 km to 248 km, showing a dependence between the two objects.

During the second season (Figure 6), we observe that the trajectories of rd10, rd45, and rd50 objects were closer to the trajectory of vd24 object, whereas the trajectories of rd9 and rd52 objects were closer to the trajectory of vd115 object. Results show that distances between vd24 and rd10, vd24 and rd8, vd24 and rd45, vd115 and rd52, and vd11 and rd9 decreased in time, whereas the distance between vd24 and rd50 increased.

Figure 7 shows trajectories of selected combined vd and rd objects, called rd-vd objects. The existence of such combined objects show that regions of vd and rd objects overlap, indicating a spatial relationship between the two events.

4. Discussion

This study indicates the existence of rainfall deficit and vegetative drought events in the East African region in 1999. A qualitative analysis by visually comparing images to determine this relation is limited as it can only offer a subjective interpretation, and it can become time consuming when many images are used, for example, when analyzing a multiyear drought. Alternative approaches, while providing with quantitative analysis methods, do not consider the spatial variability of these events in a region of interest.

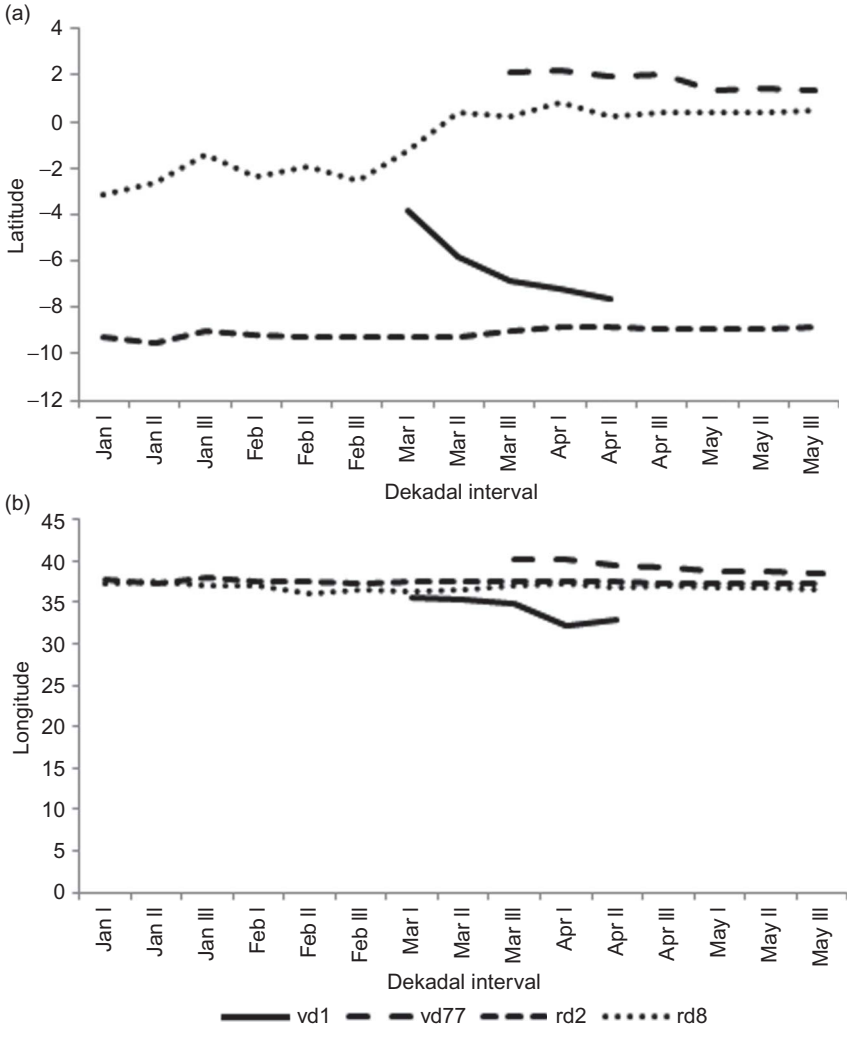

Figure 5. (a) Lat and (b) Lon coordinates of rd and vd objects plotted for the first season 1999.

Hence, they cannot propose quantitative ways to analyze their spatiotemporal dynamics within a region of interest. We propose an object-oriented analysis approach to extract entities with crisp boundaries and fuzzy (multivalues) interiors. This allows us to capture the spatiotemporal variability of values within each entity, when compared to features with crisp (single-valued) interiors. As only one category of an event, either vegetative drought or cumulative rainfall deficit, is of interest, entities can be extracted on images with crisp boundaries. The centroids are used to track the trajectory of each object. Dynomap allows us to select the size of the centroids in regard to one attribute. This approach allows us to visualize not only the movement of `vd` or `rd` objects but also the evolution of the *support-area* of these objects. Results indicate that rainfall deficits in East Africa may have caused vegetative drought in Kenya and Tanzania, as demonstrated by other studies mentioned in

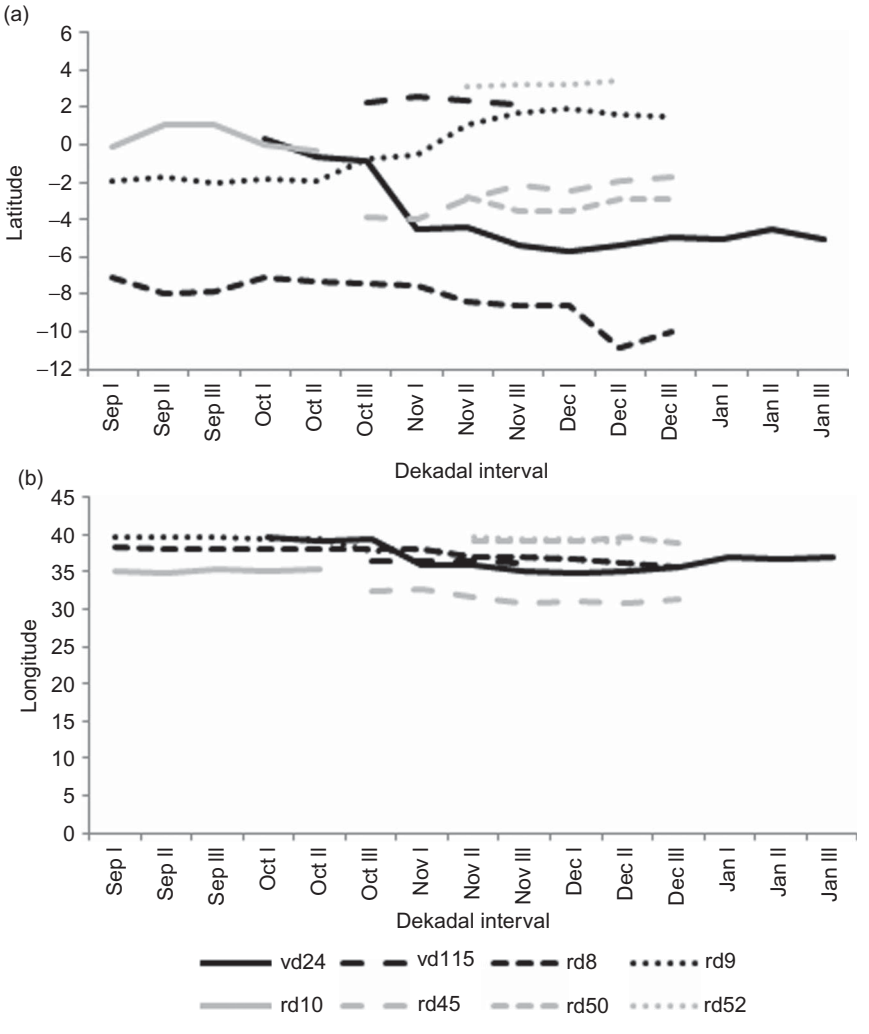

Figure 6. (a) Lat and (b) Lon coordinates of rd and vd objects plotted for the second season 1999.

Section 2.2. Visually comparing trajectories of both events show that there is a relation between them.

The use of a membership function allowed us to account for the vague nature of vegetative drought. Selection of threshold values to limit the class from NDVI anomaly values, however, remains a challenge. On the one hand, vegetative drought is characterized from NDVI anomaly values below normal. In many areas, normal conditions generally mean conditions that do not deviate from long-term averages. However, these averages themselves can change over time. Results obtained should hence be carefully interpreted, according to the long-term mean period used. On the other hand, even while considering that the normal values are unchanged, selecting a value from which a vegetative drought starts and ends is subjective. Extracting and tracking `rd` objects presented an additional challenge of segmentation, as the entities in the images are smoothed, hence spatially more connected than `vd` entities. This is caused by the modeled input data: although patches

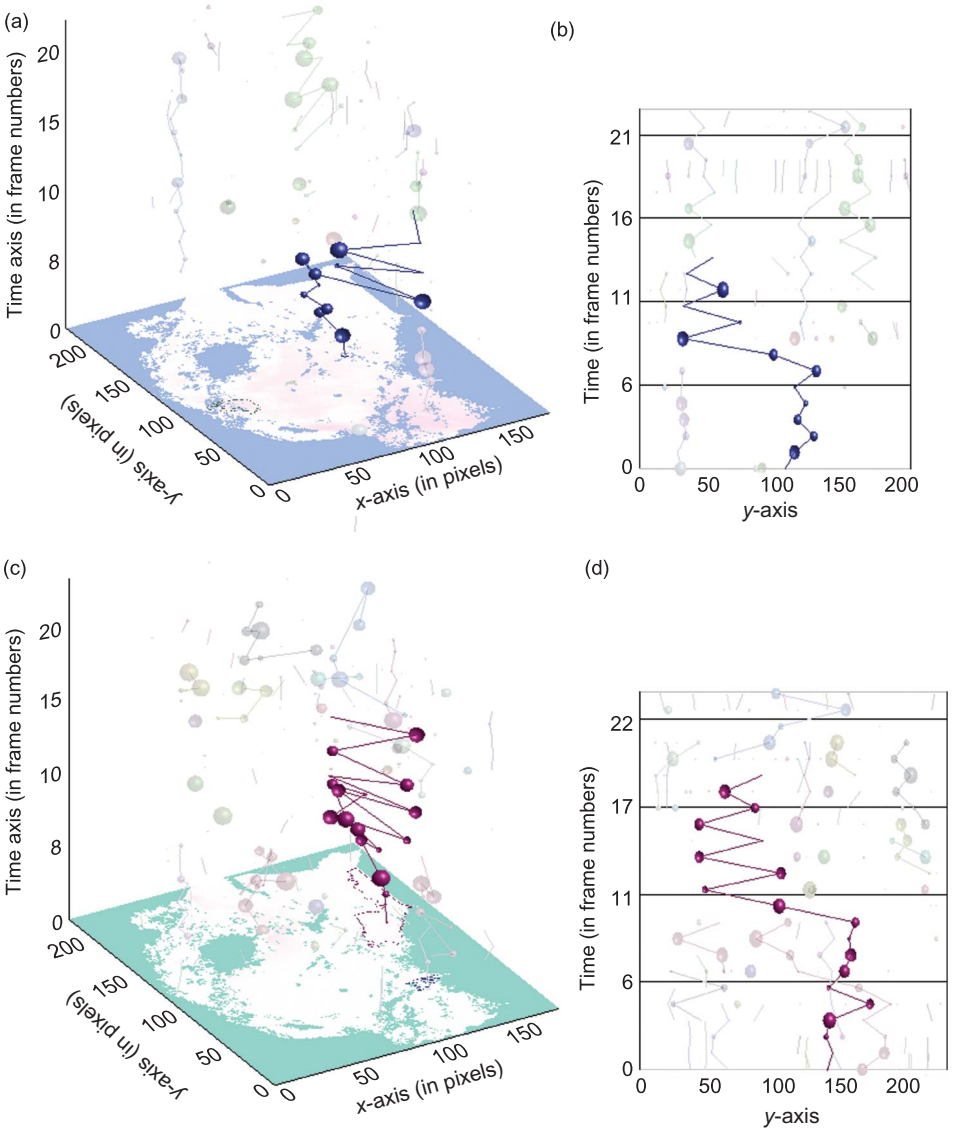

Figure 7. Trajectories of selected rd-vd objects in (a) 3D space–time cube and (b) 2D along the *y*-axis (South–North), for the first season and in (c) 3D space–time cube and (d) 2D along the *y*-axis (South–North) for the second season.

Note: Different colors represent different combined objects and different sizes represent different values of support-area of objects. Frame numbers on the time axis represent sequence numbers of dekads.

are visually separable, they are spatially connected with positive `rd` values pixels. A manual approach has been adopted here. The long-term mean values used to calculate RFE anomaly images are calculated for the years before 1999. Rainfall anomalies should then be considered relative to the long-term period used and the process of obtaining `rd` objects needs to be further developed.

The movement of vegetative drought and rainfall deficit were assessed. Quantifying their movement is a step toward increasing the accuracy of the qualitative assessment. Although a spatial relationship is observed between the two events, rainfall deficit is an important but obviously not the only source of vegetative drought. Further studies to understand the spatiotemporal movement of vegetative drought in East Africa can be carried out, such as by analyzing its possible relationship with El Niño-Southern Oscillation (ENSO) dynamics (Anyamba and Eastman 1996). Considering their centroids, spatial relationships can further be quantified for `vd` and `rd` objects using available spatial statistical methods such as using Morans' I (Moran 1950) and Mantel (Mantel and Valand 1950) tests. This may in time result in an automatic identification and tracking system that is suited for inclusion in a GIS. Results from this study are also difficult to validate using ground collected data due to the large geographical coverage of vegetative drought and its characterization. Other RS data such as that of higher spatial resolution can be used, and results can be compared for validation.

This method can be integrated into existing early warning systems, allowing for a more comprehensive monitoring and forecasting of vegetative drought. Further analysis is recommended to study the sensitivity of this method during other drought years and other drought-prone regions. This approach can further be developed by selecting for optimized vegetation stress indices, by optimizing the segmentation process of both series of objects taking into account other information, and by considering the growth cycle of vegetation of interest, in order to discriminate vegetation stress areas not caused by rainfall deficits from vegetative drought. The proposed method can also be adapted to quantify the spatiotemporal relationships between other natural geographical phenomena.

5. Conclusion

The main conclusion of this study is that object-based methods allow us to assess the trajectory of vegetative drought entities, both visually and quantitatively. Results showed that more `vd` and `rd` objects are observed during the second season 1999 when compared to the first season. This finding concides with reported literature. The higher number of `vd` compared to `rd` objects may be explained by the small patches of vegetation obtained after land-use classification. Although different `vd` objects moved in different directions and at different speed, large objects persisted in northen Kenya and northen Tanzania during both seasons. Results also showed that regions where `vd` are found coincide with those of `rd` objects, indicating the existence of a spatial relationship between vegetative drought and rainfall deficit events. This relationship is further observed with the overlapping of the two sets of objects. The use of a field-object data model allows us to take into account the spatial variation of values within each entity, which is crucial in assessing the intensity of a combined drought and rainfall pattern. Combining mathematical methods with visualization techniques gives a more effective assessment of vegetative drought, measured as multidimensional data.

References

Anyamba, A. and Eastman, J.R., 1996. Interannual variability of NDVI over Africa and its relation to El Niño/Southern Oscillation. *International Journal of Remote Sensing*, 17 (13), 2533–2548.

Blaschke, T., 2010. Object based image analysis for remote sensing. *ISPRS Journal of Photogrammetry and Remote Sensing*, 65 (1), 2–16.

Blaschke, T., Johansen, K., and Tiede, D., 2011. Object based image analysis for vegetation mapping and monitoring. *In*: Q. Weng, ed. *Advances in environmental remote sensing: sensors, algorithms, and applications*. Boca Raton, FL: CRC Press, 245–276.

Blaschke, T., Lang, S., and Hay, G., eds., 2008. *Object-bsed image analysis spatial concepts for knowledge-driven remote sensing applications series*, Lecture Notes in Geoinformation and Cartography. London: Springer.

Cheng, T., Molenaar, M., and Bouloucos, T., 1997. Identification of fuzzy objects from field observation data. *In*: C. Hirtle and A.U. Frank, eds. *Spatial information theory: a theoretical basis for GIS*, Lectures Notes in Computer Sciences, 1329. Berlin: Spring- Verlag, 241–259.

Davenport, M.L. and Nickolson, S.E., 1993. On the relation between rainfall and Normalized Difference Vegetation Index for diverse vegetation types in East Africa. *International Journal of Remote Sensing*, 14 (12), 2369–2389.

De Jong, S., Hornstra, T., and Maas, H.G., 2001. An integrated spatial and spectral approach to the classification of Mediterranean land cover types: the SSC method. *International Journal of Applied Earth Observation and Geoinformation*, 3 (2), 176–183.

Eklundh, L., 1996. *AVHRR NDVI for monitoring and mapping vegetation and drought in East Africa environments*. Thesis (PhD). Lund University.

Eklundh, L., 1998. Estimating relations between AVHRR NDVI and rainfall in East Africa at 10-day and monthly time scales. *International Journal of Remote Sensing*, 19 (3), 563–570.

FAO/GIEWS, 1999. *Food Outlook No.5 - November 1999* [online], p. 4. Available from: http://www.fao.org/docrep/004/x3582e/x3582e07.htm#P722 15990 [Accessed 11 November 2011].

Kraak, M.-J. and MacEachren, A., 1999. Visualization for exploration of spatial data. Fuest editorial of a special issue. *International Journal of Geographical Information Science*, 13, 285–287.

Mantel, N. and Valand, R.S., 1950. A technique for nonparametric multivariate analysis. *Biometrics*, 26, 547–558.

Mokhtari, A., *et al*., 2011. Monitoring the impacts of drought on land use/cover: a developed object-based algorithm for NOAA AVHRR time series data. *Journal of Applied Sciences*, 11, 3089–3103.

Moran, P.A.P., 1950. Notes on continuous stochastic phenomena. *Biometrika*, 37 (1), 17–23.

Murad, H. and Islam Saiful, A.K.M., 2011. Drought assessment using remote sensing and GIS in north-west region of Bangladesh. *In*: *3rd international conference on water & flood management (ICWFM-2011)*, Dhaka, Bangladesh.

Nicholson, S.E., Davenport M.L., and Malo, A.R., 1999. A comparison of the vegetation response to rainfall in the Sahel and East Africa, using the Normalized Difference Vegetation Index from NOAA AVHRR. *Climate Change*, 17 (2–3), 209–241.

Pinzón, J., Brown, M.E., and Tucker, C.J., 2005. Satellite time series correction of orbital drift artifacts using empirical mode decomposition. *In*: NE Huang and SSP Shen, eds, *Hilbert-Huang transform: introduction and applications*. Singapore: World Scientific Publishing Co. Pte. Ltd., 167–186.

Rulinda, C.M., *et al*., 2012. Characterising and quantifying vegetative drought in East Africa using fuzzy modeling and NDVI data. *Journal of Arid Environment*, 78, 169–178. doi:10.1016/j.jaridenv.2011.11.016.

Samtaney, R., *et al*., 1994. Visualizing features and tracking their evolution. *IEEE Computer*, 27 (7), 20–27.

Silver, D. and Wang, X., 1996. Volume tracking. *In*: R. Yagel and G. Neilson, eds., *Proceedings of the Seventh conference on IEEE Visualization (VIS'96)*, San Francisco, CA. Los Alamitos, CA: IEEE Computer Society Press, 157–164.

Sinnot, R.W., 1984. Virtues of the Haversine. *Sky and Telescope*, 68 (2), 159.

Stein, A., Hamm, N.A.S., and Qinghua, Y., 2009. Handling uncertainties in image mining for remote sensing studies. *International Journal of Remote Sensing*, 30 (20), 5365–5382.

Tucker, C.J., 1979. Red and photographic infrared linear combinations for monitoring vegetation. *Remote Sensing of Environment*, 8 (2), 127–150.

Tucker, C.J., *et al*., 2005. An extended AVHRR 8-km NDVI data set compatible with MODIS and spot vegetation NDVI data. *International Journal of Remote Sensing*, 26 (20), 4485–4498.

Turdukulov, U., 2006. Visualizing the evolution of image features in time-series: supporting the exploration of sensor data. Thesis (PhD). ITC-University of Utrecht.

Turdukulov, U.D., Tolpekin, V., and Kraak, M.-J., 2005. Visual exploration of time series of remote sensing data. *In*: *Proceedings of spatial-temporal modeling, spatial reasoning, analysis, data mining and data fusion (ISPRS-WG/II)*, 27–29 August, Beijing.

Turdukulov, U., *et al*., 2007. Connecting users with their data: an environment to explore the morphodynamics of rip channels. *Cartographica*, 42, 139–151.

UNICEF, 2000. *Drought in East Africa* [online]. Available from: http://www.unicef.org/africadrought/ [Accessed 11 November 2011].

Wang, F., 1990. Improving remote sensing image analysis through fuzzy information representation. *Photogrammetric Engineering and Remote Sensing*, 56, 1163–1169.

Xie, P. and Arkin, P.A., 1997. A 17-year monthly analysis based on gauge observations, satellite estimates, and numerical model outputs. *Bulletin of the American Meteorological Society*, 78 (11), 2539–2558.